華中科技大學

本科生毕业设计（论文）参考文献译文本

译文出处：U. Satija, B. Ramkumar and M. S. Manikandan, *"A simple method for detection and classification of ECG noises for wearable ECG monitoring devices,"* Signal Processing and Integrated Networks (SPIN), 2015 2nd International Conference on, Noida, 2015, pp. 164-169.

院　　系：光学与电子信息学院

专业班级：在这里写下你的专业名称和班级号

姓　　名：某某某

学　　号：U201200000

指导教师：某某某

2016 年 3 月

译文要求

一、 译文内容须与课题（或专业内容）联系，并需在封面注明详细出处。

二、 出处格式为

图书：作者.书名.版本（第×版）.译者.出版地：出版者，出版年.起页～止页

期刊：作者.文章名称.期刊名称，年号，卷号（期号）：起页～止页

三、 译文不少于5000汉字（或2万印刷符）。

四、 翻译内容用五号宋体字编辑，采用A4号纸双面打印，封面与封底采用浅蓝色封面纸（卡纸）打印。要求内容明确，语句通顺。

五、 译文及其相应参考文献一起装订，顺序依次为封面、译文、文献。

六、 翻译应在第七学期完成。

译文评阅

导师评语

应根据学校“译文要求”，对学生译文翻译的准确性、翻译数量以及译文的文字表述情况等做具体的评价后，再评分。

评分：_____（百分制）　　指导教师（签名）：_____

年　　月　　日

一种简单的 ECG 噪声检测与分类方法——适用于可穿戴 ECG 监测设备

摘要： 对心电图（Electrocardiogram，ECG）信号质量的评估是大多数 Holter ECG 信号和动态 ECG 信号分析应用中的第一步，也是不可或缺的一步。本文提出了一种简单的检测并分类 ECG 噪声的方法，这种方法由四个主要步骤组成：滑动平均滤波，分帧，特征提取和多级决策树算法。该方法提取了每帧信号中的动态振幅范围和最大自相关峰等特征。在第一级决策中，使用一个具有波幅依赖性的决策规则来检测低频噪声（包含基线漂移（Baseline Wander，BW）和突变干扰（Abrupt Change, ABC））以及高频噪声（包含工频干扰（Power Line Interference, PLI）和肌电干扰（Muscle Artifacts, MA））。在第二级决策中，该方法根据信号的局部动态振幅范围，进一步将低频噪声归类为 BW 噪声或 ABC 噪声，根据信号的局部最大自相关峰将高频信号分为 PLI 噪声和肌电干扰。我们使用了多种不同受干扰程度的 ECG 信号测试了该检测分类方法。结果表明，本方法的平均灵敏度可达 97.88%，效率可达 91.81%，精确度可达 89.06%。

1 简介

近年来，可穿戴式心脏保健监测让我们能够不间断地记录 ECG 信号，并使心血管疾病得到尽早地发现和治疗。一般来说，常见的 ECG 信号振幅为 10μV 至 5mV，而其频率介于 0.05-150Hz 之间。ECG 信号记录普遍受到噪声干扰，即基线飘移，工频干扰，肌电干扰以及设备噪声干扰。另外，运动伪影干扰在基于无线体域网（WBANs）的 ECG 监测中也十分普遍。从图 1 所示的受干扰 ECG 信号中，我们可以注意到 BW，PLI 以及肌电干扰造成了 ECG 特征点、特征测量、心率分段等项目的测量不准确。因此，ECG 信号质量评估已成为大多数 Holter ECG 信号和动态 ECG 信号分析应用中的第一步，同时也是不可或缺的一步，这些应用包括心律失常识别、心率变异分析、基于 ECG 的生物特征识别、每搏心跳间血压的不间断测量以及睡眠呼吸暂停检测等。另外，信号质量评估不仅显著提高了心血管疾病诊断系统的准确性，也能帮助我们挑选出适当的 ECG 信号增强技术。然而，可穿戴 ECG 监测设备虽然保证了信号的持续纪录以及心脏疾病的提早发现，但其电量、电池寿命、计算能力和存储器大小均为有限。所以，在选择适当的噪声削减技术时，可穿戴设备需要的是低耗能的噪声检测和分类手段，并借此保证所记录的 ECG 信号的临床可接受性。

1.A 对 ECG 信号质量评估方法的回顾

根据相关研究报告，多数信号质量评估（Signal Quality Assessment, SQA）方法均基于如平均数、标准差、峰度及启发式规则的统计特性。在参考文献 4 中，Orphanidou 等人提出了针对 QRS 信号和 PPG（PhotoPlethysmoGraphy）信号的一种信号质量衡量方法：先使用启发式规则检测 QRS 或 PPG 脉冲中提取出的特征、RR 间期、最大和最小 RR 间期的比值，再进行模板匹配。参考文献 5 提出了一种通过人工重建目标导联来评估信号质量的方法，其步骤包括 LF 与 HF 噪声移除、能量下凹指数分析、使用神经网络程序估算出 ECG 导联间的相关性。参考文献 6 中，L. Johannesen 和 L. Galeotti 等人提出了一种自动为 ECG 质量评分的方法。这种方法通过分析导联丢失、检测 QRS 波、对 QRS 波分割、检测错误的 QRS 波来排除 ECG 中的宏大误差，再对 BW、PLI 和肌电干扰加以量化。在参考文献 7 中，D. Hayn 等人提出了基于 QRS 检测的 ECG 质量评估标准，其中包括对空载导联的检测，尖峰检测，导联信号交叉点检测以及 QRS 检测的鲁棒性。

参考文献 8 中提出了一些用于确定临床可接受性的信号质量指标和数据融合方法，包括谱能分布、高阶矩、通道间和算法间协议、多层神经网络和支持向量机。文献 9 中提出了一种使用经验模态分析和统计学方法来自动探测运动伪影和噪声干扰的方式。文献 10 中 Hayn 等人提出了针对移动医疗应用中患者增权的 ECG 质量评估方法。这种方法分析了信号的基本特征（振幅，尖峰，常数信号部分等）、不同导联间的交叉点个数以及 QRS 振幅与噪声振幅的比值。文献 11 中 B.E.Moody 提出了一种基于条件的 ECG 信号质量控制。文献 12 提出了一种基于 Android 平台的 ECG 质量评估，能够探测所有导联中的失效导联、全局高频噪声、造成 QRS 探测问题的含噪声导联、全局低频噪声以及窦性搏动中的高低频噪声。文献 13 中，Liu 等人提出了使用手机处理所收集的 ECG 数据的实时信号质量评估方法。这种方法能够通过检测四种标志性事件来判别四种错误：电极的错误放置，强脉冲，强高斯噪声和基于模版匹配的 R 波波峰探测算法造成的错误。通过对这四种标志性事件的检测，该方法能分别计算出单个导联的单一信号质量指数和 12 个导联的整体信号质量指数。文献 14 提出了 Android 平台上评估 ECG 信号质量的简易评分系统。文献 15 中提出了一种评估正常状态和噪声所致衰减的动脉血压信号质量指数。大多数现有的方法都使用了 PICC2011（Physionet/Computing in Cardiology Challenge 2011）所提供的数据。

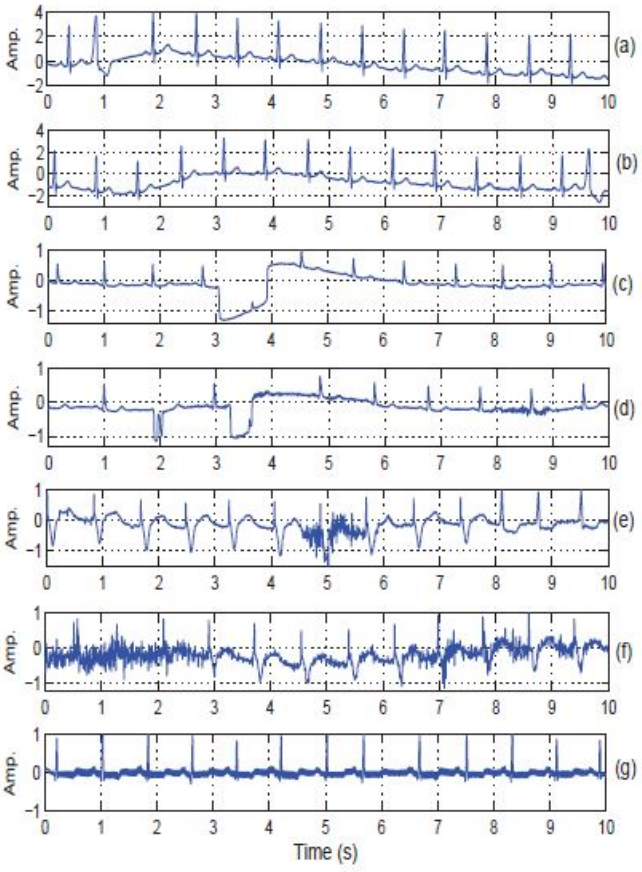

图 1: 图中的 ECG 信号掺入了不同类型的噪声及伪影：(a) 和 (b) 中 ECG 信号受基线漂移影响，(c) 和 (d) 中 ECG 信号受突变干扰，(e) 和 (f) 中 ECG 信号受肌电干扰，(g) 中 ECG 信号受 PLI 噪声干扰。

1.B 现有 SQA 方法的局限性

许多基于 QRS 信号检测的 SQA 方法都源于对输入 ECG 信号中探测到的 RR 间期的分析。当无噪声 ECG 信号记录包含以下成分时，RR 间期的精确测量将收到严重干扰：（1）宽 QRS 波群；（2）低振幅 QRS 波群；（3）负极性的 QRS 波群；（4）RR 间期中的突变；（5）QRS 波的振幅突变；（6）QRS 波形态的突变；（7）尖锐的 P 波和 T 波。在这些情况下，现有的使用心率评估 ECG 信号质量的方法要求能够对 ECG 信号中出现的 R 峰进行精确的实时测量。大多数方法采用传统的 R 峰检测（或波形描绘）算法，这些算法应用于 ECG 信号时检测率很低。此外，大多数检测方法包含了一系列用于检测 R 峰的振幅阈值、持续时间阈值和间期长度阈值，这些阈值要么忽略了噪声，要么计入了噪声，最后错过了 R 峰。一种包含适当的振幅阈值和时间阈值的前向搜索算法被广泛应用于采纳或抛弃 t_m 和 t_n 之间已检测到的 R 峰：（1）$t_n - t_m < 0.2s$（不应期）；（2）$t_n - t_m > 1.5RR_{avg}$ 时向前搜索。这些条件或许能提高对于规律性节律的探测，但其中一些条件可能相互冲突。此外，前向搜索机制在检测含

有变化 QRS 波群的非规律性节律时不能被终止。还有，启发式规则中往往含有大量阈值设定。大多数方法中，这些用于检测的阈值是基于之前检测到的 R 峰设定的。这样，检测方法的性能就极大地依赖于对学习阶段中初始阈值的估计是否精确。

基于 EMD 的方法将局部波形中的 ECG 信号和噪声分离成一系列固有模态函数方程（Intrinsic Mode Functions, IMFs）。这时，从信号 IMF 中确定出噪声 IMF 就很困难。虽然每一个小波子带的频率范围是已知的，但 BW、PLI、MA 所致噪声以及 ECG 信号的小波系数被分入了细节子带和近似子带中。因此，在 PQRST 波的形态和噪声的特点均随时间变化时，噪声子带的特征难以确定。然而，我们并不能纠正小波滤波器、分解层数和特征子带，因此建立一种低复杂度的 ECG 信号质量自动评估方法仍然是一个具有挑战性的研究课题。

1.C　本文的贡献

本文提出了一种简单直接的 ECG 噪声监测和分类方法。我们提出的方法分为四个主要步骤：滑动平均滤波，分帧，特征提取和多级决策分类。该方法中，一些如全局 / 局部动态振幅和最大自相关峰等特征被提取出来。在这些特征的基础上，多级决策被建立起来并用于自动检测和分类 ECG 噪声。实验结果表明该方法在检测各种不同类型的带噪 / 非带噪信号时的分类准确性均为可接受的。本文的组织结构介绍如下：第二部分描述了所提出的 ECG 噪声检测和分类方法；第三部分介绍了使用多种带噪 / 非带噪 ECG 信号测试并验证所提出方法的性能。最后，第四部分得出了结论。

2　ECG 噪声检测与分类方法

在这部分中，我们提出了一种简单直接的方法来检测和分类 ECG 噪声。这种方法由四部分组成：信号抑制及噪声增强，特征提取，振幅检测，还有基于决策树的噪声分类。

2.A　信号抑制和噪声增强

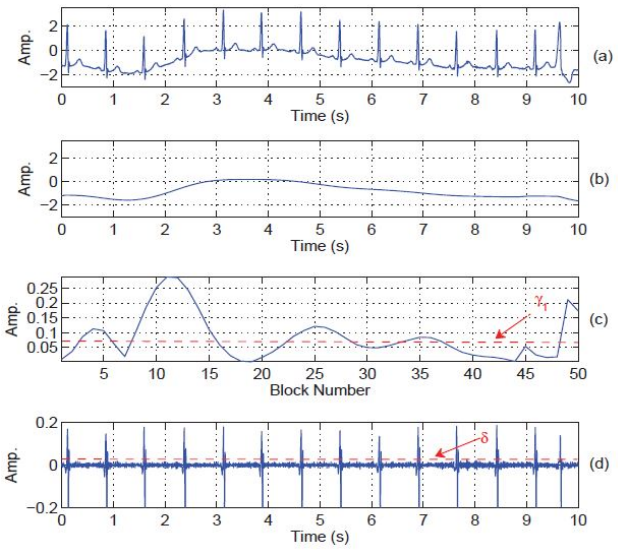

图 2: 从带 BW 噪声 ECG 信号中获取的特征信号。(a) 为受干扰 ECG 信号，(b) 为提取得到的带 BW 噪声低频组分，(c) 为动态振幅范围估计，(d) 为高频组分。

该过程中，我们提出的方法使用了滑动平均滤波器来提取低频噪声组分（包含 BW 噪声）和高频噪声组分（包括 PLI 噪声，MA 噪声和记录设备噪声）。滤波步骤处理了 10s 的 ECG 信号 $x[n]$。用于将输入 ECG 信号中 BW 噪声（或低频噪声伪影）提取出来的滑动平均滤波器可表示如下：

$$\mathbf{u}[n] = \frac{1}{L+1}\sum_{k=0}^{L}\mathbf{x}[n-k] \qquad (1)$$

这里 L 表示滑动平均滤波器的长度。该过程中，选取这样的滤波器长度是为了让其足以捕捉到 0.5Hz 以下的 BW 噪声。同时，用于将输入 ECG 信号中的高频噪声（包括 PLI 噪声，MA 噪声以及记录设备噪声）提取出来的滤波器差分方程如下：

$$\mathrm{v}_1[n] = \frac{1}{L+1}\sum_{k=0}^{L}\mathbf{x}[n-k] \qquad (2)$$

$$\mathrm{v}[n] = \mathrm{x}[n] - \mathrm{v_l}[n],\ \ n = 0, 1, 2....., N-1 \tag{3}$$

第二个滑动平均滤波器长度的选取依据是令其足以捕捉 40Hz 以下的 ECG 信号。为了避免相位滞后，滤波操作采用了零相位滤波器（滤波器系数为 $b_k = 1,\ \ k = 0, 1, 2, 3....., L-1$）。之后，通过检测 BW，PLI，MA 以及记录设备噪声的出现来提取低频组分和高频组分中的噪声信号特征。图 2(b) 及 (d) 中的输出波形展示了从带噪 ECG 信号中获取的低频和高频组分。

2.B 特征提取

特征提取通过以下两个步骤实现：非重叠分帧和特征计算。在分帧过程中，经过滤波的信号被分为了非重叠的帧，帧长 200ms。在这个过程中，信号 $\mathbf{u}[n]$ 中第 k 帧 $\mathbf{u}_k[n]$ 由以下算式给出：

$$\mathbf{u}_k[n] = \mathbf{u}[\mathrm{P}k + n]\ \ n = 1, 2, ...\mathrm{P} \tag{4}$$

此处 $k = 0, 1...\mathrm{M}-1, \mathrm{M} = \lfloor \frac{\mathrm{N}}{\mathrm{P}} \rfloor$，P 表示帧长。通过计算每帧中振幅的最大最小值来鉴别出掩盖了 PQRST 波形中低振幅局域波的背景噪声。该过程中，每帧中的最大最小振幅值由如下算式计算得出：

$$\begin{aligned} a_{\max}[k] &= \max\{u_k[n]\}\ \ k = 0, 1, ...\mathrm{M}-1 \\ a_{\min}[k] &= \min\{u_k[n]\}\ \ k = 0, 1, ...\mathrm{M}-1 \end{aligned} \tag{5}$$

通过比较每帧信号的动态振幅范围和预设的振幅阈值，BW 噪声可以被探测到。动态振幅范围由以下算式给出：

$$a_{\mathrm{dr}}[k] = a_{\max}[k] - a_{\min}[k]\ \ k = 0, 1, 2, ...\mathrm{M}-1 \tag{6}$$

特征提取中每个步骤的输出波形见图 2。图 2(b) 中的低频组分包含了振幅出现大幅波动的 BW 噪声。为了将 BW 噪声和突变伪影区分开来，该方法估算了每帧信号的局部动态振幅范围。低频组分中，对动态振幅范围进行估算后的输出结果如图 2(c)。通过设置预设的振幅阈值条件 $\gamma_1, a_{\mathrm{dr}}[k] > \gamma_1$，检测得具有较低振幅帧数比率的 BW 噪声被与突变伪影区分开来。

表 1: ECG 局部波类型及其特征

ECG 波类型	振幅范围	持续时间
P 波	0.1-0.2mV	100ms
QRS 波群	0.5-1.0mV	80-100ms
T 波	$\approx$ 0.5mV	150-200ms
U 波	1-2mm 或 T 波振幅的 25%	-

对于高频噪声（如 PLI 和 MA 噪声）的检测，首先通过公式3提取信号的高频组分 $\mathbf{v}(n)$。滤波器的阶数被设定为能够正确捕获高频组分中 50/60Hz 的 PLI 噪声和肌电干扰噪声。以用于测试的含 BW 噪声 ECG 信号为处理对象，从中提取的高频组分如图 2(d) 所示。经观测，高频组分中不仅含有低振幅高频噪声，也含有部分 QRS 波群信号。在这一步处理过程中，通过比较高频组分振幅的最大绝对值和预设的振幅阈值 δ，高频噪声的影响程度得以确定。而该振幅阈值的确定则依赖于 ECG 信号中局部波形的各项振幅值（见表1）。基于这些局部波振幅值，振幅阈值得以选定。低振幅的 PLI 噪声和肌电干扰噪声或许能通过一个简单的平滑滤波器去除。该方法假设高振幅值的 PLI 和肌电干扰噪声能够掩盖住中等振幅值局部波（包括 P，Q，T，U 波）的关键点（如起始点，终止点和峰值点）。若能使用这种噪声消除技术恢复关键点，则这时的噪声水平被认为是可接受的。振幅阈值 δ 的选择值为 0.02mV。至于高频噪声的探测，我们估算了振幅值大于 $\delta = 0.02\mathrm{mV}$ 的采样点的总数 ($\mathrm{N_{HF}}$)。如果估算的 $\mathrm{N_{HF}} > 2 \times \mathrm{F_s}$，则算法认为存在高频噪声。

一旦确定了高频噪声确实存在，高频噪声将会被进一步分类为 PLI 噪声和肌电干扰噪声。

在高频噪声分类程序中，高频组分经过了重叠分帧，帧长为200ms，帧移 Q 为 100ms。重叠分帧的方法可表达为：

$$\mathbf{v}_k[n] = \mathbf{v}[\frac{\mathrm{P}k}{2} + n] \quad n = 1, 2, ...\mathrm{P} \quad (7)$$

其中 $k = 0, 1, ...\mathrm{M}_1 - 1$，且 $\mathrm{M}_1 = \lfloor \frac{N}{Q} \rfloor$。在本部分处理中，利用自相关性将 PLI 结构噪声和肌电干扰噪声分离。在我们之前的研究中，使用自相关函数来确定信号的周期被证明是有效的。对于每帧信号 $\mathbf{v}_k[n]$，自相关序列计算如下：

$$\mathbf{R}_k(\tau) = \frac{1}{P}\sum_{n=0}^{\mathrm{P}} \mathbf{v}_k[n]\mathbf{v}_k[n+\tau] \quad (8)$$

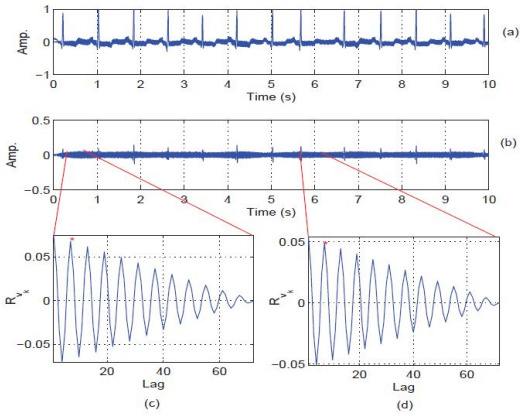

图 3: 从带 PLI 噪声的高频组分中获取的帧信号表消除了周期性。(a) 为带 PLI 噪声的 ECG 信号，(b) 为提取所得带 PLI 噪声的高频组分仍包含了 ECG 中的 QRS 波群高频部分。(c) 为第一个 R 峰与第二个 R 峰之间的采样帧中的交流信号；(d) 为第八个 R 峰和第九个 R 峰之间的交流信号。

其中 $\mathbf{R}_k(\tau)$ 表示 $\mathbf{v}_k[n]$ 的自相关函数（Autocorrelation Function, ACF），τ 表示自相关函数的延迟时间。通过参考第一个负过零点（由正到负的过零点称为负过零点，译者注），每帧中自相关函数的局部最大值能够被估算出来。图 3 表示出了自相关函数的结果，以便观察。自相关图谱显示 PLI 结构噪声是存在的。ACF 的有效性也进一步通过处理含有肌电干扰和 PLI 噪声的 ECG 信号进行了评估。自相关性提取的输出波形见图 4，图 5。对于这两个带噪 ECG 信号，低频组分示意图显示出了振幅值小于振幅阈值 δ 的 BW 噪声组分。含 PLI 与 MA 噪声的 ECG 信号高频组分分别见图 4(d) 和图 5(d)。ACF 特征信号见图 4(e) 和图 5(e)。从图 4(e) 的 ACF 信号中可看出多数帧中，信号的峰值小于 0.2。该实验中，我们注意到大多数帧肌电干扰信号的帧内相关性不显著。同时，图 5(e) 中的 ACF 结果显示大多数帧中的信号峰值大于 0.4。通过选择一个合适的自相关峰阈值，高频组分能够被分为 PLI 噪声和肌电干扰噪声。一种简单的多级决策噪声检测和分类方法如图 6 所示。

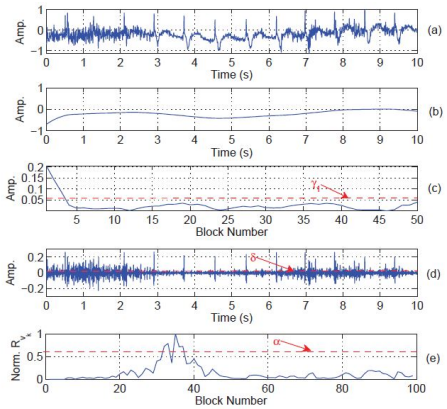

图 4: 受肌电干扰的 ECG 的特征提取。(a) 受干扰的 ECG；(b) 提取出的带 BW 的低频组分；(c) 动态振幅范围估算；(d) 高频组分；(e) 最大自相关峰方法提取的自相关函数特征。

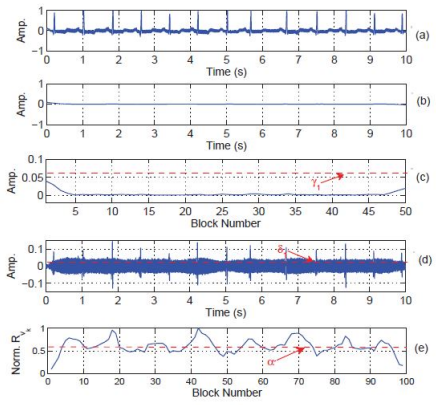

图 5: 带 PLI 噪声 ECG 的特征提取。(a) 受干扰 ECG 信号；(b) 带 BW 噪声的低频组分；(c) 动态振幅范围评估；(d) 高频组分；(e) 使用最大自相关峰提取的自相关函数特征。

3 结果与讨论

在这部分中，我们评估了所提出的噪声检测分类方法的性能，用于评测的 ECG 信号包含了不同形态的 PQRST 波，其中包括了 BW 噪声、ABC 噪声，PLI 噪声和肌电干扰噪声等多种噪声。在本研究中，第一个决策阶段首先检测了低频噪声（BW 噪声和 ABC 噪声）和高频噪声（PLI 噪声和肌电干扰噪声）是否存在。在第二个决策阶段，低频组分和高频组分被归类为 BW 噪声、ABC 噪声，PLI 噪声和肌电干扰这几类。该 ECG 噪声检测归类方法的简易流程图见图 6。

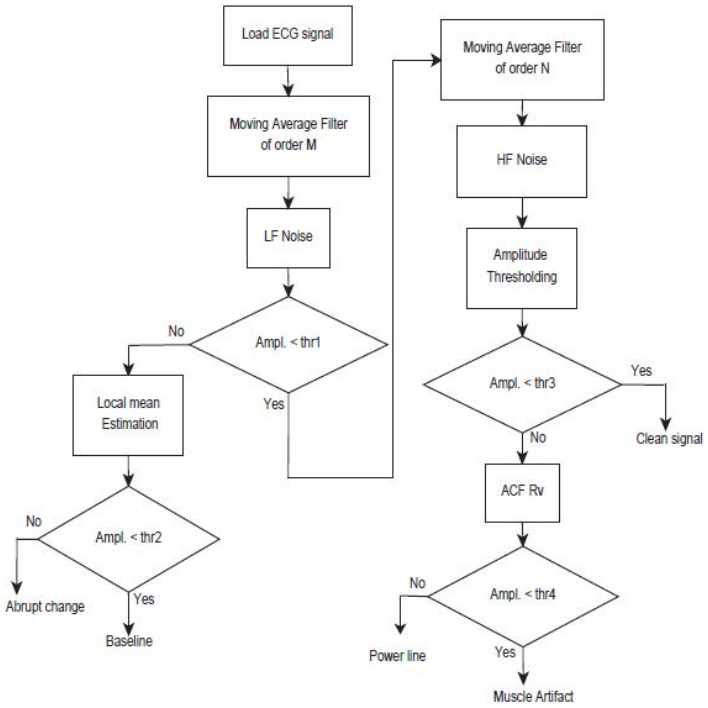

图 6: 本文中 ECG 噪声检测和分类方法的简易流程图

对于性能评估方法，使用 MIT-BIH 心律失常数据库（MIT-BIH Arrhythmia Database，mitadb）中的 ECG 记录构建了大规模 ECG 测试信号数据库。这些 ECG 信号的采样率为 360Hz，分辨率为 11-bit。ECG 测试信号数据库共含有 150 条 ECG 信号记录。每个 ECG 测试信号的记录时常为 10s。大规模 ECG 测试信号数据库中的信号加入了各种不同噪声级别的噪声。这些合成的噪声通过文献 21 中的软件包生成。分类结果与真实数据的对比见表2。

性能测试中，灵敏度 Se，效率 +P 和精确度三种测试评分计算如下：

$$Se = \frac{\mathrm{TP}}{\mathrm{TP} + \mathrm{FN}} \times 100 \tag{9}$$

$$+\mathrm{P} = \frac{\mathrm{TP}}{\mathrm{TP} + \mathrm{FP}} \times 100 \tag{10}$$

$$Accuracy = \frac{\mathrm{TP}}{\mathrm{TP} + \mathrm{FN} + \mathrm{FP}} \times 100 \tag{11}$$

其中 TP（True Positive）表示算法正确分类了测试片段，FP（False Positive）表示算法将测试片段错误地分为了某类噪声，FN（False Negative）表示测试片段所含的噪声类型分类错误。表4总结了本文所提出方法的测试评分结果。对于大部分类型的噪声（除了 ABC、PLI 混合噪声以及 ABC、MA 混合噪声），该方法的分类准确度达到了 85% 以上。表3给出了本分类方法

表 2: 噪声检测分类算法结果与真实结果比较

波形记录	真实情况								
	非带噪信号	BW	ABC	MN	PL	BW+PL	BW+MN	ABC+PL	ABC+MN
100	9	66	21	5	23	1	25	0	0
101	2	74	9	0	4	14	43	2	2
102	4	68	23	0	26	0	29	0	0
103	6	74	16	15	23	1	15	0	0
104	3	41	7	5	5	10	73	0	6
105	6	66	18	0	24	2	34	0	0
106	19	55	13	15	18	6	21	0	3
107	18	111	8	0	5	8	0	0	0
108	4	23	18	1	4	11	86	0	3
109	11	72	19	16	17	1	14	0	0
111	4	77	7	6	7	15	33	0	1
总数	86	727	159	63	156	69	373	2	15
波形记录	算法分类结果								
	非带噪信号	BW	ABC	MN	PL	BW+PL	BW+MN	ABC+PL	ABC+MN
100	8	62	25	6	20	4	24	1	0
101	3	85	15	0	2	10	34	0	1
102	8	70	25	3	20	5	15	1	1
103	4	71	20	21	21	5	8	0	0
104	2	34	5	8	3	8	81	0	9
105	9	61	15	1	28	3	32	0	1
106	17	51	15	15	20	8	23	0	1
107	20	108	11	4	4	3	0	0	0
108	1	15	14	9	3	10	91	1	6
109	14	75	17	14	14	1	15	0	0
111	2	82	10	8	3	11	34	0	0
总数	88	714	172	89	138	68	357	3	21

表 3: 本文中分类方法的混淆矩阵

	非带噪信号	BW	ABC	MN	PL	BW+PL	BW+MN	ABC+PL	ABC+MN
非带噪信号	86	2	-	-	-	-	-	-	-
BW	3	714	-	2	-	-	8	-	-
ABC	-	3	159	-	-	-	6	-	4
MN	-	-	4	63	2	-	14	-	6
PL	-	-	-	7	138	9	-	2	-
BW+PL	-	-	-	-	-	68	1	-	-
BW+MN	-	-	-	8	-	-	357	-	8
ABC+PL	-	-	-	1	-	-	-	2	-
ABC+MN	-	-	-	-	-	-	5	1	15

表 4: 本文方法的分类结果

信号类型	信号片段数量	TP	FP	FN	Se(%)	+P(%)	准确度 (%)
非带噪信号	86	86	2	-	100	97.72	97.72
BW	727	714	-	13	98.21	100	98.21
ABC	159	159	13	-	100	92.44	92.44
MN	63	63	26	-	100	92.44	92.44
PL	156	138	-	18	88.46	100	88.46
BW+PL	69	68	-	1	98.55	100	98.55
BW+MN	373	357	-	16	95.71	100	95.71
ABC+PL	2	2	1	-	100	66.66	66.66
ABC+MN	15	15	6	-	100	71.42	71.42
总数	1650	1602	48	48	97.88	91.18	89.06

的混淆矩阵。基于表4和表3的结果可以认为，我们提出的方法适用于大多数常见噪声的检测，其中包括 BW、PLI、ABC、MA 噪声，以及 BW/PLI 混合噪声、BW/MA 混合噪声。

之后，本研究将着眼于提高本文方法在检测、分类其他混合类型噪声上的性能。相较于其他现行噪声检测分类方法中的信号分离技术、特征提取技术和监督分类器，本文方法的滤波、特征提取和分类技术十分简单。而可穿戴心脏疾病监护设备由于其电量少、存储空间小、计算速率低的特点，正需要一种低复杂度的信号质量评测方法。基于我们的分类结果，我们认为本文提出的方法对于评估 Holter 和动态 ECG 信号的质量具有很高的适用性。

4 结论

本文提出了一种简单的 ECG 噪声自动检测和分类方法。这种方法由四个步骤构成：滑动平均滤波，分帧，特征提取和多级决策树算法。为了检测并分类 ECG 信号中的噪声，本方法提取了包括全局／局部动态振幅范围和最大自相关峰在内的信号特征。同时，本方法经过多种带噪／非带噪 ECG 信号输入测试并确认有效。结果表明该方法的平均灵敏度可达 97.88%，效率可达 91.18% 且准确度可达 89.06%。不同于其它现行方法，本方法的滤波、特征提取和分类方法均简单易行。

参考文献原文

A Simple Method for Detection and Classification of ECG Noises for Wearable ECG Monitoring Devices

Udit Satija, Barathram.Ramkumar and M. Sabarimalai Manikandan
School of Electrical Sciences, Indian Institute of Technology Bhubaneswar
Bhubaneswar, Odisha-751013, India.
Email:{us11,barathram,msm}@iitbbs.ac.in

***Abstract*—An assessment of electrocardiogram (ECG) signal quality has become an unavoidable first step in most holter and ambulatory ECG signal analysis applications. In this paper, we present a simple method for automatically detection and classification of ECG noises. The proposed method consists of four major steps: moving average filter, blocking, feature extraction, and multistage decision-tree algorithm. In the proposed method, the dynamic amplitude range and autocorrelation maximum peak features are extracted for each block. In the first decision stage, a amplitude-dependent decision rule is used for detecting the presence of low-frequency (LF) noise (including, baseline wander (BW) and abrupt change (ABC) artifacts) and the high-frequency (HF) noise (including, power line interference (PLI) and muscle artifacts). In the second decision stage, the proposed method further classifies the LF noise into a BW noise or a ABC noise using the local dynamic amplitude range feature. The HF noise is classified into a PLI noise or a muscle noise using the local autocorrelation maximum peak feature. The proposed detection and classification method is tested and validated using a wide variety of clean and noisy ECG signals. Results show that the method can achieve an average sensitivity (Se) of 97.88%, positive productivity (+P) of 91.18% and accuracy of 89.06%.**

I. Introduction

Recently, wearable cardiac health care monitoring devices enable continuous recording of ECG signals, and early detection and treatment of cardiovascular diseases [1], [2]. Generally, the amplitudes of a normal ECG range from 10 μV to 5 mV and the frequency lies in the range of 0.05-150 Hz [3]. The ECG recordings are generally corrupted by noises, namely, baseline wander (BW), power line interference (PLI), muscle artifact (MA) and instrumentation noise. Furthermore, the motion artifacts is ubiquitous in ECG monitoring using wireless body area networks (WBANs). From the corrupted ECG signals as shown in Fig. 1, it can be noted that the presence of BW, PLI and muscle noises causes inaccurate determination of ECG characteristic points, feature determination, heartbeat segmentation, etc. Thus, assessment of ECG signal quality has become an unavoidable first step in most holter and ambulatory ECG signal analysis applications including cardiac arrhythmias recognition, heart rate variability (HRV) analysis, ECG-based biometric, continuous beat-to-beat blood pressure measurement, sleep apnea detection, and so on. Furthermore, signal quality assessment not only plays an important role in improving diagnostic accuracy of cardiovascular diseases diagnostic systems but also plays in selecting suitable ECG signal enhancement techniques. In addition, wearable ECG monitoring devices hold the promise of continuous recording and early detection of cardiac disease events, but wearable devices have limited power and battery life, limited computational power and main memory. Thus, wearable devices demand energy-efficient reliable ECG noise detection and classification for choosing suitable noise removal technique and guaranteeing clinical acceptability of ECG recordings.

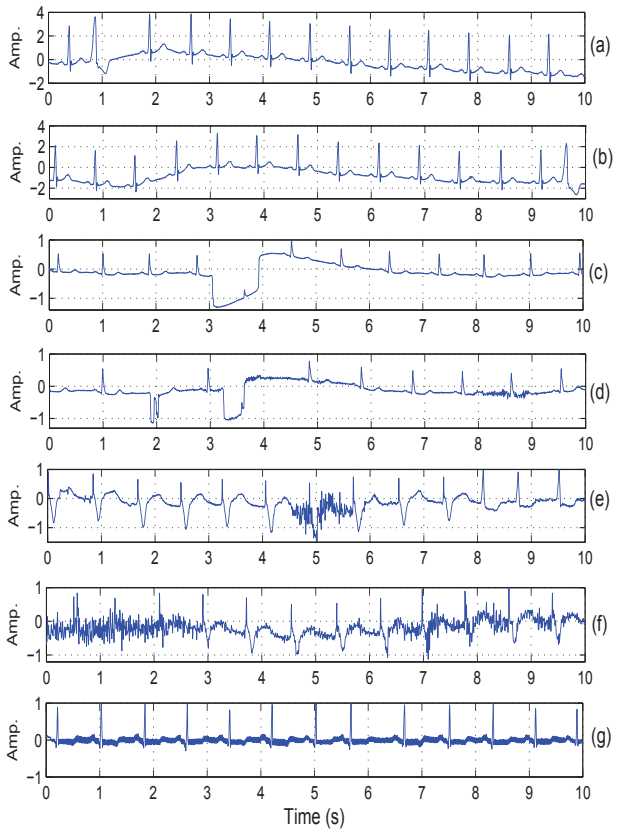

Fig. 1. Illustrates ECG signals corrupted by different types of artifacts and noise: (a) and (b) ECG corrupted with baseline wanders, (c) and (d) ECG corrupted with abrupt changing artifacts, (e) and (f) ECG corrupted with muscle artifacts, and (g) ECG corrupted with PLI noise.

A. Review of ECG Signal Quality Assessment Methods

Many signal quality assessment (SQA) methods have been reported based on statistical features such as mean, standard deviation, kurtosis and heuristic rules. In [4], Orphanidou, et al. presented signal quality indices for ECG and PPG

978-1-4799-5991-4/15/$31.00 ©2015 IEEE

signals using heuristic rules on the extracted features from the QRS or pulse portions and RR intervals, the ratio of maximum to minimum RR interval, and template matching. In [5], SQA method using an artificially reconstructed target lead is presented based on the removal of LF and HF noise, energy-concavity index (ECI) analysis, and a correlation-based examination subroutine calculated between ECG leads estimated by a suitably trained neural network. In [6], L. Johannesen and L. Galeotti presented automatic ECG quality scoring methodology. The method identifies ECG signals with macroscopic errors and subsequently quantifies BW, PLI or muscular noise based on the missing leads, QRS detection, segmentation and erroneous QRS detection. In [7], D. Hayn et al. presented QRS detection based ECG quality assessment based on the empty lead criterion, spike detection criterion, lead crossing point criterion and robustness of QRS detection.

In [8], signal quality indices (SQIs) and data fusion methods were presented for determining clinical acceptability of ECGs. The method consists of spectral energy distribution, higher order moments and inter-channel and inter-algorithm agreement, multi-layer perceptron (MLP) artificial neural network and support vector machine (SVM). In [9], automatic motion and noise artifact detection was presented using empirical mode decomposition (EMD) and statistical approaches. In [10], Hayn et al. presented ECG quality assessment for patient empowerment in m-Health applications. The method is based on basic signal properties (amplitude, spikes, constant signal portions), number of crossing points in between different leads, and QRS amplitude vs. noise-amplitude ratio. In [11], B. E. Moody presented rule-based methods for ECG quality control. In [12], assessment of ECG quality on an android platform was performed based on the lead-fail in all leads, global high frequency noise, leads with noise causing QRS detection problems, global low frequency noise and low and high frequency noise in the beats of sinus origin. Liu et al. presented real-time signal quality assessment for ECGs collected using mobile phones [13]. The method is based on the four flags: misplaced electrode, huge impulse, strong Gaussian noise, error of R-wave peaks by the template matching. Based on the values of four flags, single signal quality index (SSQI) and integrative signal quality index (ISQI) were computed for single lead ECG and twelve-lead ECGs, respectively. In [14], simple scoring system for ECG quality assessment on android platform. In [15], a new ABP signal quality index (SQI) was presented for measuring morphological normality and degradation due to noise. Most existing SQA methods were validated using datasets available in Physionet/Computing in Cardiology Challenge 2011 (PICC2011) [18].

B. Limitations of Existing SQA Methods

Many QRS detection based SQA methods were proposed by analyzing the detected R-R intervals from the input ECG signal. The detection of exact R-R interval (or heart rate) is severely affected in the cases of clean ECG signal with (i) wide QRS complexes, (ii) low-amplitude QRS complexes, (iii) negative QRS polarities, (iv) sudden changes in RR intervals, (v) sudden changes in QRS amplitudes, (vi) sudden changes in QRS morphologies, and (vii) sharp P- and T-waves [22],[23]. Under this scenarios, the existing heart rate ECG signal quality assessment methods demand accurate detection of time-instants of R-peaks present in the ECG signal. Most methods use traditional R-peak detection (or waveform delineation) algorithm, which had poor detection rates in case of ECG signals. Furthermore, most detection methods include sets of amplitude-dependent, duration-dependent and interval-dependent thresholds for to detect R-peaks, and to reject or include noise and missed R-peaks. The searchback algorithm with two rules with adaptive amplitude-dependent and time-dependent thresholds were widely adopted to reject or include identified R-peaks located at t_m and t_n: $i)$ if $t_n - t_m < 0.2\ s$ (refractory period) and $ii)$ search back if $t_n - t_m > 1.5\mathrm{RR}_{\mathrm{avg}}$. These rules may improve detections for regular rhythms but some rules may be in conflict with others. Furthermore, searchback mechanism cannot be halted in case of irregular rhythms with varying QRS complexes. Moreover, there are often lots of thresholds defined in heuristic rules [22]. In most approaches, the detection thresholds were adapted based on past detected R-peaks. In such a case, detection performance highly depends on the accurate estimation of initial thresholds at the learning phase.

In EMD based methods, local waves of ECG signal and noises are distributed over a number of intrinsic mode functions (IMFs). Under this scenario, it is difficult to determine the noisy IMFs from the signal IMFs. Although the frequency range of each wavelet subband is known, the wavelet coefficients of BW, PLI, and MA noises and ECG signal are spread over detail and approximation subbands. Thus, noise subband characterization can be difficult under time-varying PQRST morphologies and noise characteristics. However, we cannot fix the wavelet filter, number of decomposition level and characteristic subbands. Thus, developing low-complexity automated ECG signal quality assessment method is still a challenging research problem.

C. Contribution of this Paper

In this paper, we present a simple straightforward ECG noise detection and classification method. The proposed method consists of four major stages: moving average filtering, blocking, feature extraction, and multi-stage decision classification. In the proposed method, the features such as global and local dynamic amplitudes and autocorrelation maximum peak are extracted in this work. Based on these features, the multi-stage decision stage is constructed automatic detection and classification of ECG noises. Experimental results show that the method achieves an acceptable classification accuracy on different types of clean and noisy ECG signals.

The rest of this paper is organized as follows. The proposed ECG noise detection and classification method is described in Section II. In Section III, the performance of the proposed method is tested and validated using a wide variety of clean and noisy ECG signals. Finally, conclusions are drawn in Section IV.

II. Proposed ECG Noise Detection and Classification Method

In this Section, we present a simple straightforward method for automatically detection and classification of ECG noises. The proposed method consists of four major stages: signal suppression and noise enhancement, feature extraction, amplitude-dependent detection and decision-tree based noise classification.

A. ECG Signal Suppression and Noise Enhancement

In this work, the proposed method implements a moving average filter for obtaining the low-frequency (LF) component part including the BW noises and the high-frequency (HF) component part including the PLI, muscle artifacts and recording instrument noise. In this work, the filtering step process the 10 s ECG signal $x[n]$. For extracting the baseline wander noise (or low-frequency (LF) artifacts) from the input ECG signal, the moving average filter is implemented as

$$\mathbf{u}[n] = \frac{1}{L+1}\sum_{k=0}^{L}\mathbf{x}[n-k] \tag{1}$$

where L denotes the moving average filter length. In this work, the filter length is chosen such that it can adequately capture the BW noise below 0.5 Hz. The high-frequency (HF) noise including the PLI, muscle artifacts and recording instrument noise from the input ECG signal is extracted using the difference equation as

$$\mathrm{v}_1[n] = \frac{1}{L+1}\sum_{k=0}^{L}\mathbf{x}[n-k] \tag{2}$$

$$\mathrm{v}[n] = \mathrm{x}[n] - \mathrm{v}_1[n], \qquad n = 0, 1, 2....., N-1. \tag{3}$$

The filter length for the moving average filter II is chosen such that it can adequately capture the ECG signal below 40 Hz. In order to avoid phase lags, the filtering operation is implemented using zero-phase filtering process with filter coefficients $b_k = 1, \quad k = 0, 1, 2, 3, ...L-1$. Then, the noise signal features are extracted from both LF component and HF component parts for detecting the presence of BW, PLI, muscle artifacts and recording instrument noises. The output waveforms as shown in Fig. 2 (b) and (d) show the LF component and HF component parts obtained for the ECG signal corrupted with BW noise.

B. Feature Extraction Stage

The feature extraction stage is implemented based on the following steps: non-overlapping blocking and feature computation. In the blocking process, the filtered signal is divided into non-overlapping blocks with block duration of 200 ms. In this work, the kth block $\mathbf{u}_k(n)$ of $\mathbf{u}(n)$ is obtained as

$$\mathbf{u}_k[n] = \mathbf{u}[\mathrm{P}k+n] \quad n = 1, 2, \cdots \mathrm{P} \tag{4}$$

where $k = 0, 1 \cdots \mathrm{M}-1$, $\mathrm{M} = \lfloor \frac{\mathrm{N}}{\mathrm{P}} \rfloor$ and P denotes the size of the window. For each processing window, the maximum and minimum values are computed for discriminating the background noise level which can mask the low-amplitude local waves of the PQRST morphologies. In this work, the maximum and minimum amplitude values of each window are computed as

$$\begin{aligned} a_{\max}[k] &= \max\{u_k[n]\} \quad k = 0, 1 \cdots \mathrm{M}-1 \\ a_{\min}[k] &= \min\{u_k[n]\} \quad k = 0, 1 \cdots \mathrm{M}-1 \end{aligned} \tag{5}$$

For detecting the presence of BW noises, the dynamic amplitude range of each window is compared with the predefined amplitude threshold. The dynamic amplitude range is computed as

$$a_{\mathrm{dr}}[k] = a_{\max}[k] - a_{\min}[k] \quad k = 0, 1, 2 \cdots \mathrm{M}-1 \tag{6}$$

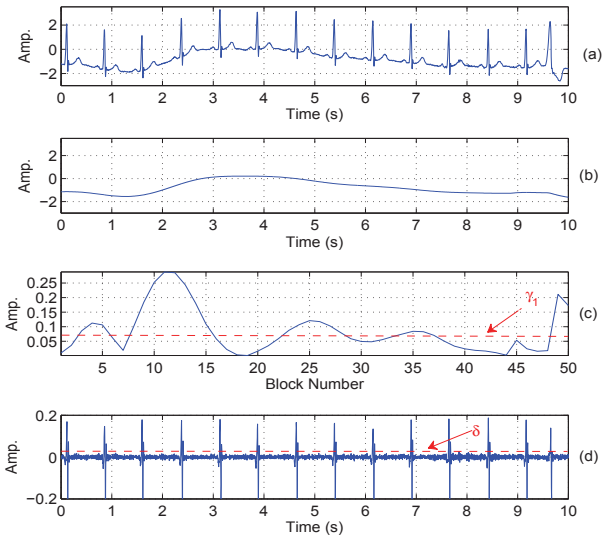

Fig. 2. Illustrates the feature signals obtained for the ECG signal with BW noise. (a) Corrupted ECG signal, (b) Extracted LF component part including BW noise, (c) dynamic amplitude range estimates, and (d) high-frequency (HF) component part.

The output waveforms of each step of the feature extraction stage are shown in Fig. 2. The LF component part in Fig. 2(b) contains the BW noise with larger amplitude variation. In order to discriminate the BW noise from the abrupt change artifacts, the local dynamic amplitude range is estimated for each window. The output of the dynamic amplitude range estimator for the LF component part is shown in Fig. 2 (c). By implementing the amplitude thresholding rule with a predefined threshold γ_1, $a_{dr}[k] > \gamma_1$, the BW noise event is distinguished from the abrupt change artifacts by determining low-magnitude frame ratio.

TABLE I. ECG LOCAL WAVES AND THEIR CHARACTERISTIC PARAMETERS [19], [20]

ECG Waves	Amplitude Range	Duration
P wave	0.1-0.2 mV	100 ms
QRS complex	$0.5 - 1.0$ mV	$80 - 100$ ms
T wave	≈ 0.5 mV	$150 - 200$ ms
U wave	$1 - 2$ mm or 25 % of T wave height	-

For detecting the presence of HF noise components such as PLI and muscle noises, the HF component part $\mathbf{v}(n)$ is obtained using equation (3). The order of the filter is chosen such that the 50/60 Hz PLI and muscle noises are captured in the HF component part. For a test ECG signal corrupted with BW noise, the extracted HF component part is shown in Fig. 2(d). It is observed that the HF component not only contains low-amplitude high-frequency background noise but also includes components of QRS complexes. In this work, the influence of the high-frequency noises is first detected by comparing the estimated maximum value of the absolute of HF component with a predefined amplitude threshold δ, which is found based on the amplitudes of local waves of the ECG signal as shown in Table I. Based upon the amplitudes of local waves, the amplitude threshold δ is chosen. The low-amplitude PLI and muscle noises may be removed by

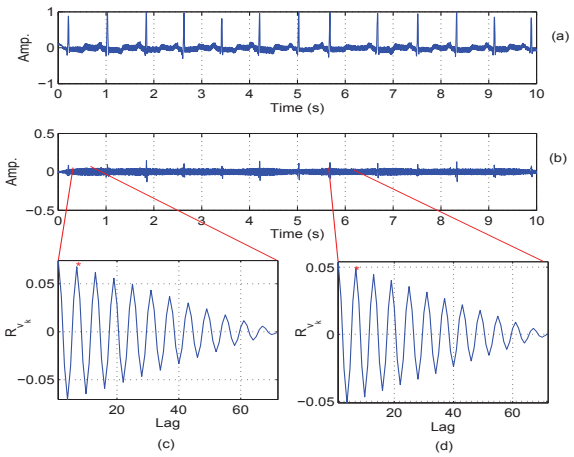

Fig. 3. Illustrates the existence of periodicity of the signal block obtained from the HF component part including the PLI noise. (a) ECG signal corrupted with PLI noise, (b) Extracted HF component including the PLI noise and high-frequency component of the QRS complexes in the ECG signal, (c) AC sequence obtained for block of samples taken from between first R-peak and second R-peak, and (d) AC sequence obtained for the eighth and ninth R-peaks.

using a simple smoothing filter. The method assumes that the high-amplitude PLI and muscle noises can mask the fiducial points (onsets, offsets, peaks) of the medium amplitude local waves (including, P, q, T, and U). In this work, the acceptable background noise level is chosen such that the fiducial points can be preserved after applying noise removal techniques. The amplitude threshold δ of 0.02 mV is chosen. For detecting the presence of HF noise part, we estimate the total number of samples ($\mathrm{N_{HF}}$) that are above the δ=0.02 mV. If the estimated $\mathrm{N_{HF}} > 2 \times \mathrm{F}_s$ then the method labels the presence of HF noise part.

Once the presence of the HF noise part is identified then the HF noise is further processed to classify the HF noise part into a PLI noise or a muscle noise. In the HF noise classification process, the HF component part is segmented into overlapping blocks with duration of 200 ms with block shift (Q) of 100 ms. The overlapping blocking process is implemented as

$$\mathbf{v}_k[n] = \mathbf{v}[\frac{\mathrm{P}k}{2} + n] \quad n = 1, 2, \cdots \mathrm{P} \tag{7}$$

where $k = 0, 1 \cdots \mathrm{M}_1 - 1$ and $\mathrm{M}_1 = \lfloor \frac{\mathrm{N}}{\mathrm{Q}} \rfloor$. In this work, the autocorrelation features are used for discriminating the structured PLI noise from the muscle noise. In our previous work, the effectiveness of the autocorrelation function in determining the periodicity of the signal [24]. For each block $\mathbf{v}_k[n]$, the autocorrelation sequence is computed as

$$\mathbf{R_k}(\tau) = \frac{1}{\mathrm{P}} \sum_{n=0}^{\mathrm{P}} \mathbf{v}_k[n]\mathbf{v}_k[n+\tau] \tag{8}$$

where $\mathbf{R_k}(\tau)$ denotes the autocorrelation function (ACF) for $\mathbf{v}_k[n]$ and τ denotes the autocorrelation lag. With reference to the first negative zerocrossing point, the global maximum of the autocorrelation function is estimated for each block. The results of the autocorrelation function are shown in Fig. 3 for visual inspection. The autocorrelation plots show that

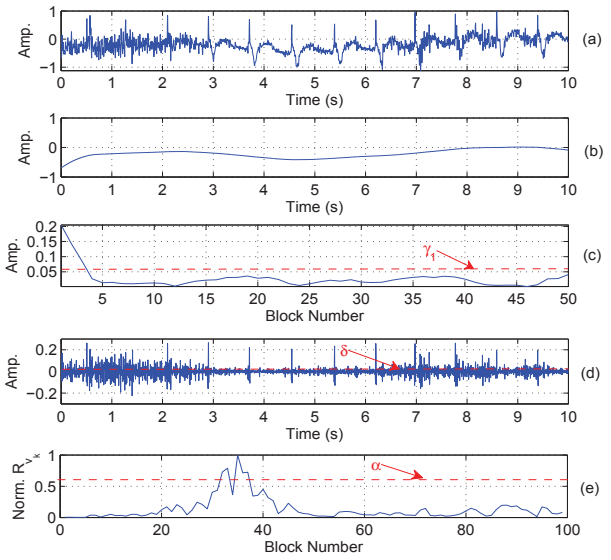

Fig. 4. Illustrates the feature signals obtained for the ECG signal with muscle artifacts. (a) Corrupted ECG signal, (b) Extracted LF component part including BW noise, (c) dynamic amplitude range estimates, (d) high-frequency (HF) component part and (e) ACF feature signal obtained using maximum peak value of the ACF function.

the existence of the structured PLI noise. The effectiveness of the ACF function is further evaluated using the ECG signals corrupted with muscle artifacts and PLI noise. The output waveforms of the autocorrelation feature extraction stage are shown in Figs. 4 and 5. For these two noisy ECG signals, the LF component parts show low-amplitude BW noise component which is less than the BW noise amplitude threshold γ_1. The HF component parts for the ECG signals corrupted with muscle artifacts and PLI noise are shown in Figs. 4(d) and 5(d), respectively. The ACF feature signals are shown in Figs. 4(e) and 5(e). From the ACF signal as shown in Fig. 4(e), it is noted that the most signal blocks have maximum peak value below 0.2. From this experiment, we notice that most blocks from the muscle artifact part have poor intra-block correlation. Meanwhile, the ACF result in Fig. 5(e) shows that most blocks have maximum peak value above 0.4. By selecting the suitable autocorrelation peak threshold, the HF component part is classified into a PLI noise and a muscle noise. A simplified multi-stage decision based noise detection and classification method is shown in Fig. 6.

III. Results and Discussion

In this Section, we evaluate the performance of the proposed detection and classification method using a wide variety of ECG signals including different kinds of PQRST morphologies and various kinds of artifacts and noise including baseline wander (BW), abrupt change (ABC) artifacts, power line interference (PLI) and muscle artifacts. In this work, the first decision stage first detects the presence of the low-frequency (LF) noise (including, baseline wander (BW) and abrupt change (ABC) artifacts) and the high-frequency (HF) noise (including, power line interference (PLI) and muscle artifacts). In the second decision stage, the LF component and HF component parts are further classified into any of the BW,

TABLE II. COMPARISON BETWEEN GROUND TRUTH AND THE PROPOSED CLASSIFICATION METHOD FOR DIFFERENT ECG NOISE CASES.

Record	Ground Truth Annotation									Classification Results								
	Clean	BW	ABC	MN	PL	BW+PL	BW+MN	ABC+PL	ABC+MN	Clean	BW	ABC	MN	PL	BW+PL	BW+MN	ABC+PL	ABC+MN
100	9	66	21	5	23	1	25	0	0	8	62	25	6	20	4	24	1	0
101	2	74	9	0	4	14	43	2	2	3	85	15	0	2	10	34	0	1
102	4	68	23	0	26	0	29	0	0	8	70	25	3	20	5	15	1	3
103	6	74	16	15	23	1	15	0	0	4	71	20	21	21	5	8	0	0
104	3	41	7	5	5	10	73	0	6	2	34	5	8	3	8	81	0	9
105	6	66	18	0	24	2	34	0	0	9	61	15	1	28	3	32	0	1
106	19	55	13	15	18	6	21	0	3	17	51	15	15	20	8	23	0	1
107	18	111	8	0	5	8	0	0	0	20	108	11	4	4	3	0	0	0
108	4	23	18	1	4	11	86	0	3	1	15	14	9	3	10	91	1	6
109	11	72	19	16	17	1	14	0	0	14	75	17	14	14	1	15	0	0
111	4	77	7	6	7	15	33	0	1	2	82	10	8	3	11	34	0	0
Total	**86**	**727**	**159**	**63**	**156**	**69**	**373**	**2**	**15**	**88**	**714**	**172**	**89**	**138**	**68**	**357**	**3**	**21**

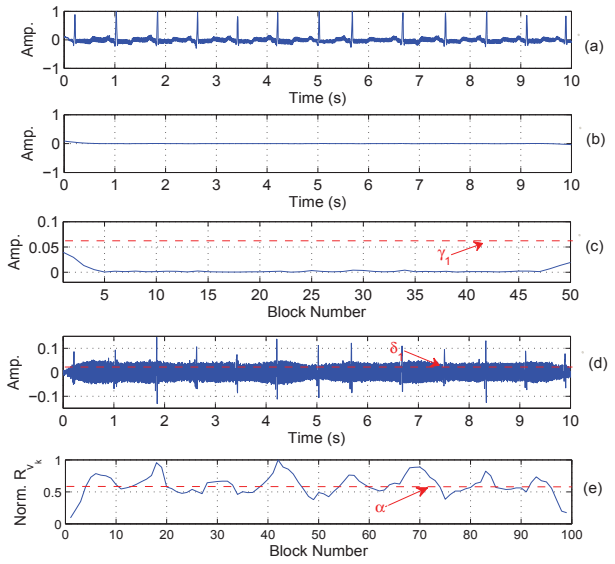

Fig. 5. Illustrates the feature signals obtained for the ECG signal with PLI noise. (a) Corrupted ECG signal, (b) Extracted LF component part including BW noise, (c) dynamic amplitude range estimates, (d) high-frequency (HF) component part and (e) ACF feature signal obtained using maximum peak value of the ACF function.

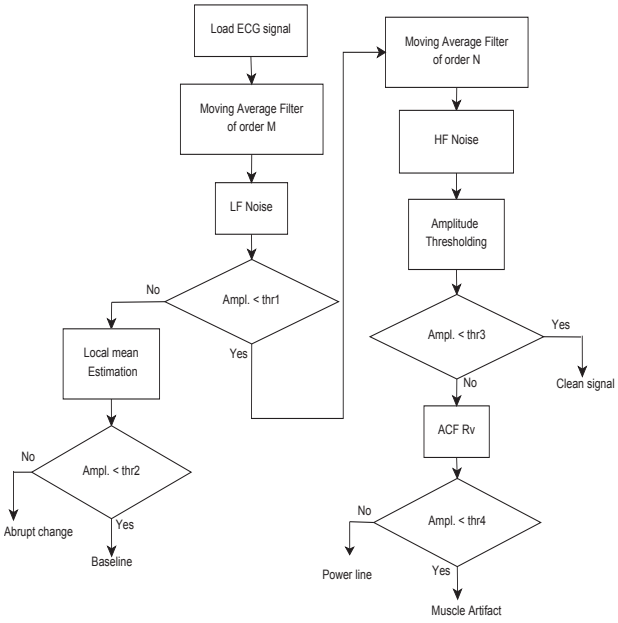

Fig. 6. A simplified flowchart of the proposed ECG noise detection and classification method.

ABC, PLI, and muscle noise classes. A simplified flowchart of the proposed ECG noise detection and classification method is shown in Fig. 6.

For performance evaluation purposes, a large scale of test ECG signal database is created using ECG signals taken from records of the MIT-BIH Arrhythmia Database (mitadb) [17]. The ECG signals were sampled at rate of 360 Hz and quantized with resolution of 11-bit. The test ECG database has 150 ECG signals. The duration of each test ECG signal is 10 s. A large scale of test ECG database is created by adding various kinds of noises with different noise levels. The synthetic noises are generated using the software package available in [21]. The ground-truth annotation results are summarized in Table II for all classes of noise.

For performance validation, the three benchmark parameters such as sensitivity (Se), positive predicitivity (+P) and accuracy are computed as

$$Se = \frac{\mathrm{TP}}{\mathrm{TP} + \mathrm{FN}} \times 100 \tag{9}$$

$$+P = \frac{\mathrm{TP}}{\mathrm{TP} + \mathrm{FP}} \times 100 \tag{10}$$

$$Accuracy = \frac{\mathrm{TP}}{\mathrm{TP} + \mathrm{FN} + \mathrm{FP}} \times 100 \tag{11}$$

where TP denotes the true positive (TP) which is defined the test segment is correctly classified by the algorithm, FP denotes the false positive defined as the the test segment is falsely classified as a particular noise type, and FN denotes the false negative defined as the test segment is misclassified as other noise type. Table III summarizes the performance of the proposed method in terms of benchmark parameters such as sensitivity (Se), positive predicitivity (+P) and accuracy. The method achieves a classification accuracy above 85% for most noise types, except for the mixture noise classes: ABC plus PLI and ABC plus muscle artifacts. The confusion matrix for the classification method is shown in Table IV. Based upon the results shown in Table III and Table IV, it is noted that the proposed method can suitable for detecting most commonly encountered noise types including BW, PLI, ABC and muscle

TABLE III. CLASSIFICATION RESULTS OF THE PROPOSED METHOD

Signal Type	**Total No. of Segments**	**TP**	**FP**	**FN**	**Se (%)**	**+P (%)**	**Accuracy (%)**
Clean	86	86	2	-	100	97.72	97.72
BW	727	714	-	13	98.21	100	98.21
ABC	159	159	13	-	100	92.44	92.44
MN	63	63	26	-	100	92.44	92.44
PL	156	138	-	18	88.46	100	88.46
BW+PL	69	68	-	1	98.55	100	98.55
BW+MN	373	357	-	16	95.71	100	95.71
ABC+PL	2	2	1	-	100	66.66	66.66
ABC+MN	15	15	6	-	100	71.42	71.42
Total	**1650**	**1602**	**48**	**48**	**97.88**	**91.18**	**89.06**

TABLE IV. CONFUSION MATRIX RESULT FOR THE PROPOSED CLASSIFICATION METHOD

	Clean	BW	ABC	MN	PL	BW+PL	BW+MN	ABC+PL	ABC+MN
Clean	86	2	-	-	-	-	-	-	-
BW	3	714	-	2	-	-	8	-	-
ABC	-	3	159	-	-	-	6	-	4
MN	-	-	4	63	2	-	14	-	6
PL	-	-	-	7	138	9	-	2	-
BW+PL	-	-	-	-	-	68	1	-	-
BW+MN	-	-	-	8	-	-	357	-	8
ABC+PL	-	-	-	1	-	-	-	2	-
ABC+MN	-	-	-	-	-	-	5	1	15

artifacts and mixture noise types including BW plus PLI, and BW plus muscle artifacts.

In the future directions, we further study the performance of the proposed detection and classification method using the other mixture of noise types. The proposed method uses simple filtering, feature extraction and classification techniques as compared with signal decomposition and feature extraction techniques and supervised classifiers of the existing noise detection and classification methods. The wearable cardiac monitoring devices highly demand a low-complexity signal quality assessment method since these wearable medical devices have limited battery power, memory space and computational speed. Based on the classification results, we believe that the proposed method is suitable for assessing the quality of ECG recordings in holter and ambulatory monitoring applications.

IV. CONCLUSION

In this paper, we present a simple method for automatically detection and classification of ECG noises. The proposed method consists of four major steps: moving average filter, blocking, feature extraction, and multistage decision-tree algorithm. In the proposed method, the features including the global and local dynamic amplitude ranges and autocorrelation maximum peak extracted for detection and classification of ECG noises. The proposed detection and classification method is tested and validated using a wide variety of clean and noisy ECG signals. Results show that the method can achieve an average sensitivity (Se) of 97.88%, positive productivity (+P) of 91.18% and accuracy of 89.06%. Unlike other existing methods, the proposed method uses simple filtering, feature extraction and classification techniques.

REFERENCES

[1] A. Pantelopoulos, N. G. Bourbakis, "A survey on wearable sensor-based systems for health monitoring and prognosis," *IEEE Trans. Syst. Man Cybern. C, Appl. Rev.*, vol. 40, no. 1, pp. 1-12, 2010.

[2] S. Movassaghi, M. Abolhasan, J. Lipman, D. Smith, and A. Jamalipour, "Wireless body area networks: A survey," *IEEE Commun. Surveys Tutorials*, Accepted, 2014.

[3] P. Kligfield *et al.*, "Recommendations for the standardization and interpretation of the electrocardiogram: part I: the electrocardiogram and its technology," *J. of the American College of Cardiol.*, vol. 49, no. 10, pp. 1109-1127, 2007.

[4] C. Orphanidou, et al., "Signal quality indices for the electrocardiogram and photoplethysmogram: derivation and applications to wireless monitoring," *IEEE J. of Biomed. and Health Informatics*, 2014.

[5] H. Naseri, M. R. Homaeinezhad, "Electrocardiogram signal quality assessment using an artificially reconstructed target lead," *Computer methods in Biomechanics and Biomed. Eng.*, In press, pp. 1-16, 2014.

[6] L. Johannesen, L. Galeotti, "Automatic ECG quality scoring methodology: mimicking human annotators," *Physiological Meas.*, vol. 33, no. 9, pp. 1479-1490, 2012.

[7] D. Hayn, B. Jammerbund, and G. Schreier, "QRS detection based ECG quality assessment," *Physiological Meas.*, vol. 33, no. 9, pp. 1449-1462, 2012.

[8] G. D. Clifford, J. Behar, Q. Li, and I. Rezek, "Signal quality indices and data fusion for determining clinical acceptability of electrocardiograms," *Physiological Meas.*, vol. 33, no. 9, pp. 1419-1437, 2012.

[9] J. Lee, D. D. McManus, S. Merchant, K. H. Chon, "Automatic motion and noise artifact detection in Holter ECG data using empirical mode decomposition and statistical approaches," *IEEE Trans. on Biomed. Eng.*, vol. 59, no. 6, pp. 1499-1506, 2012.

[10] D. Hayn, B. Jammerbund, G. Schreier, "ECG quality assessment for patient empowerment in mHealth applications." *Comput. Cardiol.*, pp. 353-356, Sept. 2011.

[11] B. E. Moody, "Rule-based methods for ECG quality control," *Comput. Cardiol.*, vol. 38, pp. 361-3, 2011.

[12] L. Johannesen, "Assessment of ECG quality on an android platform," *38th Physionet Cardiol. Challenge*, 2011.

[13] C. Liu, P. Li, L. Zhao, F. Liu, and R. Wang, "Real-time signal quality assessment for ECGs collected using mobile phones," *IEEE Comput. Cardiol.*, pp. 357-360, Sep. 2011.

[14] V. Chudacek, L. Zach, J. Kuzilek, J. Spilka, and L. LhotskA, "Simple scoring system for ECG quality assessment on android platform," *Comput. Cardiol*, pp. 449-451, Sep. 2011.

[15] Q. Li, R. G. Mark, and G. D. Clifford, "Artificial arterial blood pressure artifact models and an evaluation of a robust blood pressure and heart rate estimator," *Biomed. Eng. online*, vol. 8, no. 1, 2009.

[16] S. J. Redmond, N. H. Lovell, J. Basilakis, and B. G. Celler, "ECG quality measures in telecare monitoring," *Eng. Medicine and Biology Soc., 2008. EMBS 2008. 30th Annual Int. Conf. IEEE*, pp. 2869-2872, Aug. 2008.

[17] http://physionet.org/physiobank/database/mitdb/

[18] http://physionet.org/challenge/2011/

[19] J. R. Hampton, "The ECG Made Easy," *Elsevier Health Sciences*, 2013.

[20] R. M. Rangayyan, "Biomedical signal analysis," *IEEE Standards Office*, 2001.

[21] P.E. McSharry, G.D. Clifford, ECGSYN-a realistic ECG waveform generator (http://www.physionet.org/physiotools/ecgsyn/

[22] P. Kathirvel, M. Sabarimalai Manikandan, S. R. M. Prasanna, and K. P. Soman, "An efficient R-peak detection based on new nonlinear transformation and first-order Gaussian differentiator," *Cardiovascular Eng. and Technology*, vol. 2, no. 4, pp. 408-425, 2011.

[23] M. Sabarimalai Manikandan and B. Ramkumar, "Straightforward and robust QRS detection algorithm for wearable cardiac monitor," *Healthcare Technology Lett.*, vol. 1, no. 1, pp. 40-44, 2014.

[24] M. S. Manikandan, and K. P. Soman, "Robust heart sound activity detection in noisy environments," *Elect. Lett.*, vol. 46, no. 16, pp. 1100-1102, 2010.